

## 1308 **Classical Cyclotron**

1309 **Abstract** This chapter introduces the classical cyclotron, and the theoretical material  
1310 needed for the simulation exercises. It begins with a brief reminder of the historical  
1311 context, and continues with beam optics and with the principles and methods which  
1312 the classical cyclotron leans on, including  
1313 - ion orbit in a cyclic accelerator,  
1314 - weak focusing and periodic transverse motion,  
1315 - revolution period and isochronism,  
1316 - voltage gap and resonant acceleration,  
1317 - the cyclotron equation.

1318 The simulation of a cyclotron dipole will either resort to an analytical model of the  
1319 field: the optical element DIPOLE, or will resort to using a field map together with  
1320 the keyword TOSCA to handle it and raytrace through. An additional accelerator  
1321 device needed in the exercises, CAVITE, simulates a local oscillating voltage. Run-  
1322 ning a simulation generates a variety of output files, including the execution listing  
1323 zgoubi.res, always, and other zgoubi.plt, zgoubi.CAVITE.out, zgoubi.MATRIX.out,  
1324 etc., aimed at looking up program execution, storing data for post-treatment, produc-  
1325 ing graphs, etc. Additional keywords are introduced as needed, such as the matching  
1326 procedure FIT[2]; FAISCEAU and FAISTORE which log local particle data in  
1327 zgoubi.res or in a user defined ancillary file; MARKER; the 'system call' command  
1328 SYSTEM; REBELOTE, a 'do loop'; and some more. This chapter introduces in addi-  
1329 tion to spin motion in accelerator magnets; dedicated simulation exercises include a  
1330 variety of keywords: SPNTRK, a request for spin tracking, SPNPRT or FAISTORE,  
1331 to log spin vector components in respectively zgoubi.res or some ancillary file, and  
1332 the "IL=2" flag to log stepwise particle data, including spin vector, in zgoubi.plt file.  
1333 Simulations include deriving transport matrices, beam matrix, optical functions and  
1334 their transport, from rays, using MATRIX and TWISS keywords.

1335 **Notations used in the Text**

$B; B_0$	magnetic field; at a reference radius $R_0$
$\mathbf{B}; B_R; B_y$	field vector; radial component; axial component
$BR = p/q$	magnetic rigidity
$C; C_0$	orbit length, $C = 2\pi R$ ; reference, $C_0 = 2\pi R_0$
$E$	ion energy, $E = \gamma m_0 c^2$
$f_{\text{rev}}, f_{\text{rf}}$	revolution and RF voltage frequencies
$G$	gyromagnetic anomaly, $G = 1.7928$ for proton, $-4.184$ for helion
$h$	harmonic number, an integer, $h = f_{\text{rf}}/f_{\text{rev}}$
$k = \frac{R}{B} \frac{dB}{dR}$	radial field index
$m; m_0; M$	ion mass; rest mass; in units of $\text{MeV}/c^2$
$\mathbf{p}; p; p_0$	ion momentum vector; its modulus; reference
$q$	ion charge
$R; R_0; R_E$	equilibrium orbit radius; reference, $R(p_0)$ ; at energy $E$
$RF$	Radio-Frequency
1336 $s$	path variable
$T_{\text{rev}}, T_{\text{rf}}$	revolution and accelerating voltage periods
$\mathbf{v}; v$	ion velocity vector; its modulus
$V(t); \hat{V}$	oscillating voltage; its peak value
$W$	kinetic energy, $W = \frac{1}{2}mv^2$
$x, x', y, y'$	radial and axial coordinates $\left[ (*)' = \frac{d(*)}{ds} \right]$
$\alpha$	trajectory deviation, or momentum compaction
$\beta = \frac{v}{c}; \beta_0; \beta_s$	normalized ion velocity; reference; synchronous
$\gamma = E/m_0c^2$	Lorentz relativistic factor
$\Delta p, \delta p$	momentum offset
$\varepsilon_u$	Courant-Snyder invariant ( $u : x, r, y, l, Y, Z, s, \text{etc.}$ )
$\theta$	azimuthal angle
$\phi$	RF phase at ion arrival at the voltage gap

1337 **2.1 Introduction**

1338 Cyclotrons are the most widespread type of accelerator, today, used by thousands,  
 1339 with the production of isotopes as the dominant application. This chapter is devoted  
 1340 to the first cyclic accelerator: the early 1930s *classical* cyclotron which its concept  
 1341 limited to low energy, a few 10s of  $\text{MeV}/\text{nucleon}$ . This limitation overcome a decade  
 1342 later by the azimuthally varying field (AVF) technique, this is the subject of the next  
 1343 chapter.

1344 The classical cyclotron is based on four main principles:

1345 (i) the use of a cylindrical-symmetry magnetic field in the gap of an electromagnet  
 1346 (Fig. 2.1) to maintain ions on a circular trajectory

- 1347 (ii) transverse vertical confinement of the beam obtained by a slow radial decrease  
 1348 of the magnetic field. A technique known as weak focusing, applied over the years  
 1349 in all cyclic accelerators: microtron, betatron, synchrocyclotron, synchrotron. These  
 1350 weak focusing accelerator species all are still part of the landscape today  
 1351 (iii) resonant acceleration by synchronization of a fixed-frequency accelerating volt-  
 1352 age on the quasi-constant revolution time (Fig. 2.1). and  
 1353 (iv) use of high voltage, to mitigate the effect of the turn-by-turn RF phase slip.

1354 Resonant acceleration has the advantage that a small gap voltage is enough to  
 1355 accelerate with, in principle, no energy limitation, by contrast with the electrostatic  
 1356 techniques developed at the time, which required the generation of the full voltage,  
 1357 such as the Van de Graaf which was limited by sparking at a few tens of megavolts.

1358 The cyclotron concept goes back to the late 1920s [1], yet it was not until the early  
 1359 1930s when a cyclotron was first brought to operation [2]. The principles are sum-  
 1360 marized in Fig. 2.1: an oscillating voltage is applied on a pair of electrodes (“dees”)  
 1361 forming an accelerating gap and placed between the two poles of an electromagnet.  
 1362 Ions reaching the gap during the acceleration phase of the voltage wave experience  
 1363 an energy boost; no field is experienced inside the dees. Under the effect of energy  
 1364 increase at the gap every half-revolution, they spiral out in the quasi-constant field  
 of the dipole.

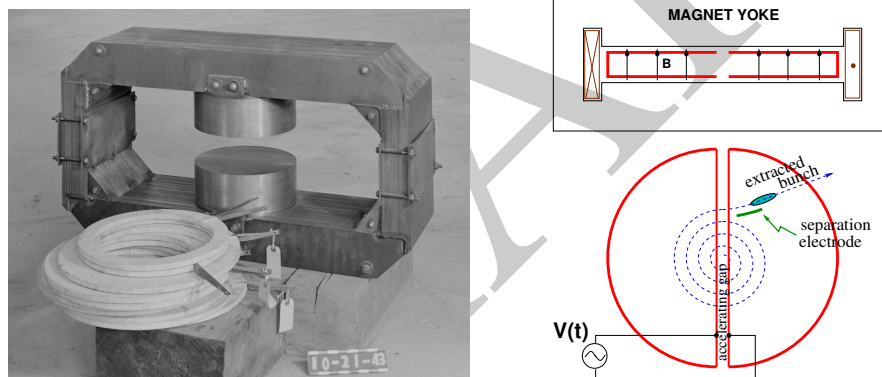


**Fig. 2.1** Left: a cyclotron electromagnet, namely here that used for a model of Berkeley’s 184-inch cyclotron in the early 1940s [3]. Magnetic field in the gap decreases with radius. Right: a schematic of the resonant acceleration motion; gap after gap, accelerated ions spiral out (bottom) in the quasi-uniform field (top). A double-dee (or, a variant, a single-dee facing a slotted electrode) forms an accelerating gap. The fixed-frequency oscillating voltage  $V(t)$  applied is a harmonic of the revolution frequency. Ions experiencing proper voltage phase at the gap, turn by turn, are accelerated. A septum electrode allows beam extraction

1365 The first cyclotron achieved acceleration of  $H_2^+$  hydrogen ions to 80 keV [2], at  
 1366 Berkeley in 1931. The apparatus used a dee-shaped electrode vis-à-vis a slotted  
 1367 electrode forming a voltage gap, the ensemble housed in a 5 in diameter vacuum  
 1368 chamber and placed in the 1.3 Tesla field of an electromagnet. A  $\approx 12$  MHz vacuum  
 1369 tube oscillator provided 1 kVolt gap voltage.  
 1370

1371 One goal foreseen in developing this technology was the acceleration of protons  
 1372 to MeV energy range for the study of atom nucleus. And in background, a wealth  
 1373 of potential applications. An 11 in cyclotron followed which delivered a  $0.01 \mu\text{A}$   
 1374  $\text{H}_2^+$  beam at 1.22 MeV [4], and a 27 in cyclotron later reached 6 MeV (Fig. 2.2) [5].  
 1375 Targets were mounted at the periphery of the 11-inch cyclotron, disintegrations were  
 1376 observed in 1932. And, in 1933: *'The neutron had been identified by Chadwick*  
 1377 *in 1932. By 1933 we were producing and observing neutrons from every target*  
 1378 *bombarded by deuterons.'* [5, M.S. Livingston, p. 22].

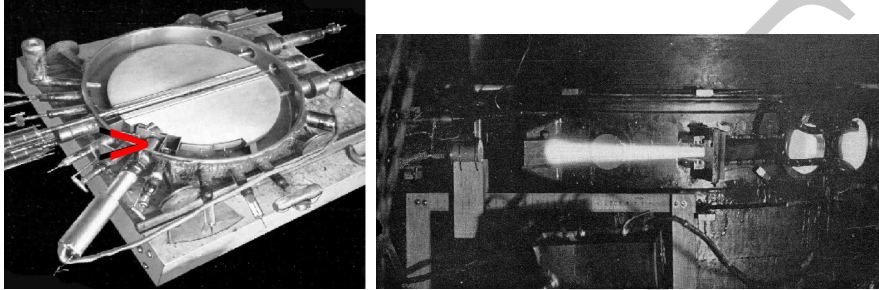
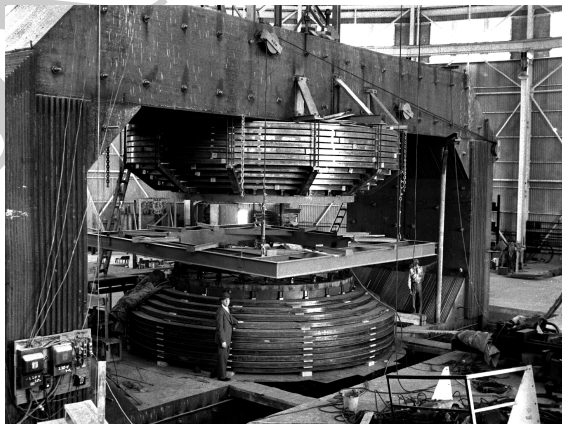


**Fig. 2.2** Berkeley 27-inch cyclotron, brought to operation in 1934, accelerated deuterons up to 6 MeV. Left: a double-dee (seen in the vacuum chamber, cover off), 22 in diameter, creates an accelerating gap: 13 kV, 12 MHz radio frequency voltage is applied for deuterons for instance (through two feed lines seen at the top right corner). This apparatus was dipped in the 1.6 Tesla dipole field of a 27 in diameter, 75 ton, electromagnet. A slight decrease of the dipole field with radius, from the center of the dipole, ensures axial beam focusing. With their energy increasing, ions spiral out from the center to eventually strike a target (red arrow). Right: ionization of the air by the extracted beam (1936); the view also shows the vacuum chamber squeezed between the pole pieces of the electromagnet [3]

**Fig. 2.3** Berkeley 184 in diameter, 4,000 ton cyclotron during construction [3]. The coil windings around both of the magnetic poles are clearly visible. Following the invention of longitudinal focusing it was actually operated as a synchrocyclotron, in 1946. The man on the right gives the scale



1379 A broad range of applications were foreseen: “*At this time biological experiments*  
1380 *were started. [...] Also at about this same time the first radioactive tracer experiments*  
1381 *on human beings were tried [...] simple beginnings of therapeutic use, coming a*  
1382 *little bit later, in which neutron radiation was used, for instance, in the treatment*  
1383 *of cancer. [...] Another highlight from 1936 was the first time that anyone tried*  
1384 *to make artificially a naturally occurring radio-nuclide. (a bismuth isotope) [5,*  
1385 *McMillan, p. 26].*

1386 Berkeley’s 184 in cyclotron, the largest (Fig. 2.3), commissioned in 1941, was to  
1387 accelerate Deuterons to 100 MeV for meson production. It’s magnet however was  
1388 diverted to the production of uranium for the atomic bomb during the second world  
1389 war years [1]. Re-started in 1946, as a consequence of the discovery of phase focusing  
1390 the accelerator was actually operated as a synchrocyclotron (an accelerator species  
1391 addressed in Chap. 6).

### 1392 *Limitation in energy*

1393 The understanding of the dynamics of ions in the classical cyclotron took some time,  
1394 and brought two news, a bad one and a good one,

1395 (i) the bad one first: the energy limitation. A consequence of the loss of isochro-  
1396 nism resulting from the relativistic increase of the ion mass so that “[...] *it seems*  
1397 *useless to build cyclotrons of larger proportions than the existing ones [...] an accel-*  
1398 *erating chamber of 37 in radius will suffice to produce deuterons of 11 MeV energy*  
1399 *which is the highest possible [...] [6], or in a different form: “If you went to graduate*  
1400 *school in the 1940s, this inequality ( $-1 < k < 0$ ) was the end of the discussion of*  
1401 *accelerator theory” [7].*

1402 (ii) the good news now: the energy limit which results from the mass increase can  
1403 be removed by splitting the magnetic pole into valley and hill field sectors. This is  
1404 the azimuthally varying field (AVF) cyclotron technology, due to L.H. Thomas in  
1405 1938 [8]. It took some years to see effects of this breakthrough (Fig. 2.4). The AVF  
1406 is the object of Chap. 3.

1407 With the progress in magnet computation tools, in computer speed and in beam  
1408 dynamics simulations, the AVF cyclotron ends up being essentially as simple to  
1409 design and build: it has in a general manner supplanted the classical cyclotron in all  
1410 energy domains (Fig. 2.4).

## 1411 **2.2 Basic Concepts and Formulæ**

1412 The cyclotron was conceived as a means to overcome the technological difficulty of  
1413 a long series of high electrostatic voltage electrodes in a linear layout, by, instead,  
1414 repeated recirculation through a single accelerating gap in synchronism with an  
1415 oscillating voltage (Fig. 2.5). As the accelerated bunch spirals out in the uniform  
1416 magnetic field, the velocity increase comes with an increase in orbit length; the

**Fig. 2.4** Evolution of the number of the various cyclotron species, over the years [9]. From the 1950s on the AVF cyclotron rapidly supplanted the 1930s' classical cyclotron

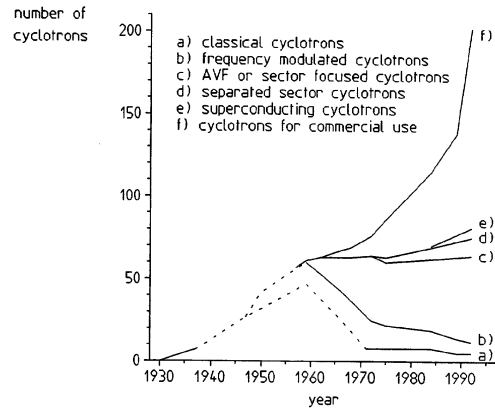


**Fig. 2.5** Resonant acceleration: in an  $h = 1$  configuration an ion bunch meets an oscillating field  $\mathbf{E}$  across gap A, at time  $t$ , at an accelerating phase; it meets again, half a turn later, at time  $t + T_{rev}/2$ , the accelerating phase across gap A', and so on: the magnetic field recirculates the bunch through the gap, repeatedly. Higher harmonic allows more bunches: the next possibility in the present configuration is  $h=3$ , and 3 bunches, 120 degrees apart, in synchronism with  $\mathbf{E}$

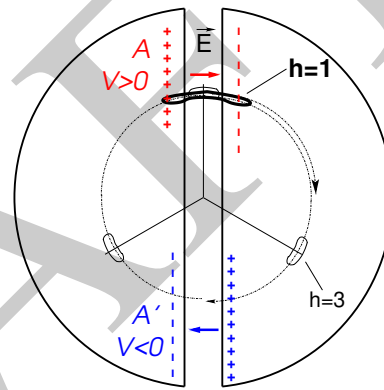
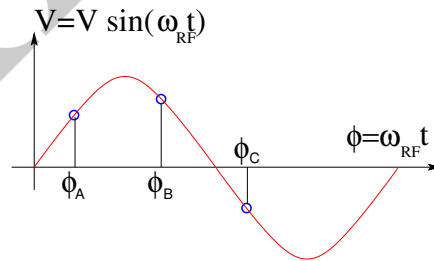


**Fig. 2.6** An ion which reaches the double-dee gap at the RF phase  $\omega_{rf}t = \phi_A$  or  $\omega_{rf}t = \phi_B$  is accelerated. If it reaches the gap at  $\omega_{rf}t = \phi_C$  it is decelerated



1417 net result is a slow increase of the revolution period  $T_{\text{rev}}$  with energy, yet, with  
 1418 appropriate fixed  $f_{\text{rf}} \approx h/T_{\text{rev}}$  the revolution motion and the oscillating voltage can  
 1419 be maintained in sufficiently close synchronism,  $T_{\text{rev}} \approx T_{\text{rf}}/h$ , that the bunch will  
 1420 transit the voltage gap at an accelerating phase (Fig. 2.6) over a large enough number  
 1421 of turns that it acquires a significant energy boost.

1422 The orbital motion quantities: radius  $R$ , ion rigidity  $BR$ , revolution frequency  
 1423  $f_{\text{rev}}$ , satisfy

$$BR = \frac{p}{q}, \quad 2\pi f_{\text{rev}} = \omega_{\text{rev}} = \frac{v}{R} = \frac{qB}{m} = \frac{qB}{\gamma m_0} \quad (2.37)$$

1424 These relationships hold at all  $\gamma$ , so covering the *classical* cyclotron domain ( $v \ll c$ ,  
 1425  $\gamma \approx 1$ ) as well as the *isochronous* cyclotron (in which the ion energy increase is  
 1426 commensurate with its mass). To give an idea of the revolution frequency, in the  
 1427 limit  $\gamma = 1$ , for protons, one has  $f_{\text{rev}}/B = q/2\pi m = 15.25 \text{ MHz/T}$ .

1428 The cyclotron design sets the constant RF frequency  $f_{\text{rf}} = \omega_{\text{rf}}/2\pi$  at an interme-  
 1429 diate value of  $hf_{\text{rev}}$  along the acceleration cycle. The energy gain, or loss, by the ion  
 1430 when transiting the gap, at time  $t$ , is

$$\Delta W(t) = q\hat{V} \sin \phi(t) \quad \text{with} \quad \phi(t) = \omega_{\text{rf}}t - \omega_{\text{rev}}t + \phi_0 \quad (2.38)$$

1431 with  $\phi$  its phase with respect to the RF signal at the gap (Fig. 2.6),  $\phi_0 = \phi(t=0)$ ,  
 1432 and  $\omega_{\text{rev}}t$  the orbital angle. Assuming constant field  $B$ , the increase of the revolution  
 1433 period with ion energy satisfies

$$\frac{\Delta T_{\text{rev}}}{T_{\text{rev}}} = \gamma - 1 \quad (2.39)$$

1434 The mis-match so induced between the RF and cyclotron frequencies is a turn-by-turn  
 1435 cumulative effect and sets a limit to the tolerable isochronism defect,  $\Delta T_{\text{rev}}/T_{\text{rev}} \approx$   
 1436  $2 - 3\%$ , or highest velocity  $\beta = v/c \approx 0.22$ . This results for instance in a practical  
 1437 limitation to  $\approx 25 \text{ MeV}$  for protons, and  $\approx 50 \text{ MeV}$  for D and  $\alpha$  particles, a limit  
 1438 however dependent on energy gain per turn.

1439 Over time multiple-gap accelerating structures were developed, whereby a  
 1440 “multiple- $\Delta$ ” electrode pattern substitutes to a “double-D”. An example is GANIL  
 1441 C0 injector with its 4 accelerating gaps and  $h = 4$  and  $h = 8$  RF harmonic opera-  
 1442 tion [10].

### 1443 2.2.1 Fixed-Energy Orbits, Revolution Period

In a laboratory frame (O;x,y,z), with (O;x,z) the bend plane (Fig. 2.7), assume  
 $\mathbf{B}|_{y=0} = \mathbf{B}_y$ , constant. An ion is launched from the origin with a velocity

$$\mathbf{v} = \left( \frac{dx}{dt}, \frac{dy}{dt}, \frac{dz}{dt} \right) = (v \sin \alpha, 0, v \cos \alpha)$$

at an angle  $\alpha$  from the  $z$ -axis. Solving

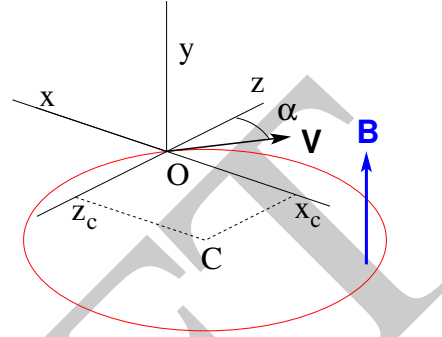


**Fig. 2.7** Circular motion of an ion in the plane normal to a uniform magnetic field  $\mathbf{B}$ . The orbit is centered at  $x_C = -v \cos \alpha / \omega_{\text{rev}}$ ,  $z_C = v \sin \alpha / \omega_{\text{rev}}$ , its radius is  $v / \omega_{\text{rev}}$

1444

$$m\dot{\mathbf{v}} = q\mathbf{v} \times \mathbf{B} \quad (2.40)$$

1445 with  $\mathbf{B} = (0, B_y, 0)$  yields the parametric equations of motion

$$\begin{cases} x(t) = \frac{v}{\omega_{\text{rev}}} \cos(\omega_{\text{rev}}t - \alpha) - \frac{v \cos \alpha}{\omega_{\text{rev}}} \\ y(t) = \text{constant} \\ z(t) = \frac{v}{\omega_{\text{rev}}} \sin(\omega_{\text{rev}}t - \alpha) + \frac{v \sin \alpha}{\omega_{\text{rev}}} \end{cases} \quad (2.41)$$

1446 which result in

$$\left(x + \frac{v \cos \alpha}{\omega_{\text{rev}}}\right)^2 + \left(z - \frac{v \sin \alpha}{\omega_{\text{rev}}}\right)^2 = \left(\frac{v}{\omega_{\text{rev}}}\right)^2 \quad (2.42)$$

1447 a circular trajectory of radius  $R = v / \omega_{\text{rev}}$  centered at  $(x_C, z_C) = \left(-\frac{v \cos \alpha}{\omega_{\text{rev}}}, \frac{v \sin \alpha}{\omega_{\text{rev}}}\right)$ .

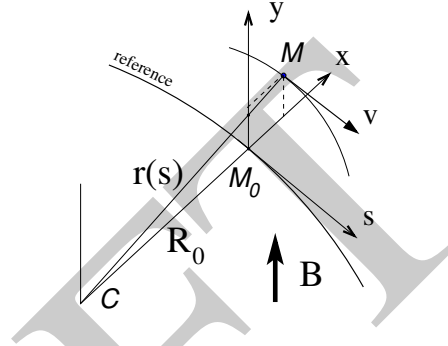
1448 *Stability of the cyclic motion* - The initial velocity vector defines a reference closed  
 1449 orbit in the median plane of the cyclotron dipole; a small perturbation in  $\alpha$  or  $v$   
 1450 results in a new orbit *in the vicinity* of the reference. An axial velocity component  $v_y$   
 1451 on the other hand, causes the ion to drift away from the reference, vertically, linearly  
 1452 with time, as there is no axial restoring force. The next Section will investigate the  
 1453 necessary field property to ensure both horizontal and vertical confinement of the  
 1454 cyclic motion in the vicinity of a reference orbit in the median plane.

### 1455 2.2.2 Weak Focusing



1456 In the early accelerated turns in a classical cyclotron (central region of the electro-  
 1457 magnet, energy up to tens of keV/u), the accelerating electric field provides vertical  
 1458 focusing for particles with proper RF phase [11, Sect. 8], whereas a flat magnetic  
 1459 field with uniformity  $dB/B < 10^{-4}$  is sufficient to maintain isochronism. Beyond  
 1460 this low energy region however, at greater radii, a magnetic field gradient must be  
 1461 introduced to ensure transverse stability: field must decrease with  $R$ .

**Fig. 2.8** Moving frame  $(M_0; s, x, y)$  along the reference circular orbit. The curvature  $1/R_0$  is constant along the orbit and  $(M_0; s, x, y)$  can be considered equivalent to the cylindrical frame  $(C; \theta, R_0, y)$



1462 Ion coordinates in the following are defined in the moving frame  $(M_0; s, x, y)$   
 1463 (Fig. 2.8), which moves along the reference orbit (radius  $R_0$ ), with its origin  $M_0$   
 1464 the projection of ion location  $M$  on the reference orbit; the  $s$  axis is tangent to the  
 1465 latter, the  $x$  axis is normal to  $s$ , the  $y$  axis is normal to the bend plane. Median-plane  
 1466 symmetry of the field is assumed, thus the radial field component  $B_R|_{y=0} = 0$  at all  
 1467  $R$  (Fig. 2.9).

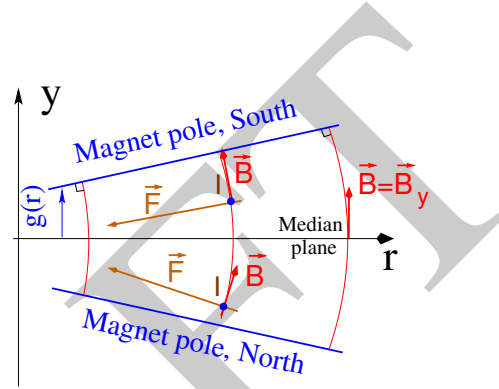
1468 Consider small motion excursions  $x(t) = r(t) - R_0 \ll R_0$ ; introduce Taylor  
 1469 expansion of the field components,

$$\begin{aligned}
 B_y(R_0 + x) &= B_y(R_0) + x \left. \frac{\partial B_y}{\partial R} \right|_{R_0} + \frac{x^2}{2!} \left. \frac{\partial^2 B_y}{\partial R^2} \right|_{R_0} + \dots \approx B_y(R_0) + x \left. \frac{\partial B_y}{\partial R} \right|_{R_0} \\
 B_R(0 + y) &= y \underbrace{\left. \frac{\partial B_R}{\partial y} \right|_0}_{= \left. \frac{\partial B_y}{\partial R} \right|_{R_0}} + \frac{y^3}{3!} \left. \frac{\partial^3 B_R}{\partial y^3} \right|_0 + \dots \approx y \left. \frac{\partial B_y}{\partial R} \right|_{R_0}
 \end{aligned} \quad (2.43)$$

1470 Using these, and noting  $(\dot{*}) = d(*)/dt$ , the linear approximation of the differential  
 1471 equations of motion in the moving frame writes

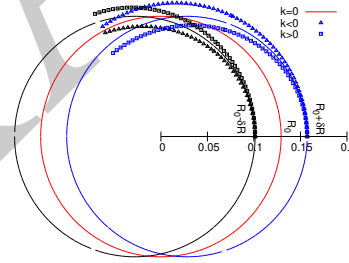
$$\begin{aligned}
 F_x = m\ddot{x} &= -qvB_y(R) + \frac{mv^2}{R_0 + x} \approx -qv \left( B_y(R_0) + \left. \frac{\partial B_y}{\partial R} \right|_{R_0} x \right) + \frac{mv^2}{R_0} \left( 1 - \frac{x}{R_0} \right) \\
 \rightarrow m\ddot{x} &= -\frac{mv^2}{R_0^2} \left( \frac{R_0}{B_0} \left. \frac{\partial B_y}{\partial R} \right|_{R_0} + 1 \right) x \quad (2.44) \\
 F_y = m\ddot{y} &= qvB_R(y) = qv \left. \frac{\partial B_R}{\partial y} \right|_{y=0} y + \text{higher order} \rightarrow m\ddot{y} = qv \frac{\partial B_y}{\partial R} y
 \end{aligned}$$

**Fig. 2.9** Axial motion stability requires proper shaping of field lines:  $B_y$  has to decrease with radius. The Laplace force pulls a positive charge with velocity pointing out of the page, at I, toward the median plane. Increasing the field gradient ( $k$  closer to -1, gap opening up faster) increases the focusing



1472

**Fig. 2.10** Geometrical focusing: take  $k=0$ ; two circular trajectories which start from  $r = R_0 \pm \delta R$  (solid lines, going counter-clockwise) undergo exactly one oscillation around the reference orbit  $r = R_0$ . A negative  $k$  (triangles), for axial focusing, decreases the radial convergence; a positive  $k$  (square markers) increases the radial convergence - and increases vertical divergence



1473

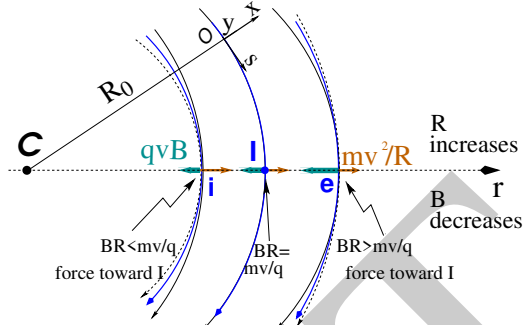
Note  $B_y(R_0) = B_0$  and introduce

$$\omega_R^2 = \omega_{\text{rev}}^2 \left( 1 + \frac{R_0}{B_0} \frac{\partial B_y}{\partial R} \right), \quad \omega_y^2 = -\omega_{\text{rev}}^2 \frac{R_0}{B_0} \frac{\partial B_y}{\partial R} \quad (2.45)$$

1474

substitute in Eqs. 2.44, this yields

**Fig. 2.11** Radial motion stability. Trajectory arcs at  $p = mv$  are represented: case of  $k = 0$  (thin black lines), of  $-1 < k < 0$  (thick blue lines), and of  $k = -1$  (dashed concentric circles).  $k$  decreasing towards  $-1$  reduces the geometrical focusing, increases axial focusing. The resultant of the Laplace and centrifugal forces,  $F_t = -qvB + mv^2/r$ , is zero at I, motion is stable if  $F_t$  is toward I at  $i$ , i.e.  $qvB_i < mv^2/R_i$ , and toward I as well at  $e$ , i.e.  $qvB_e > mv^2/R_e$



$$\ddot{x} + \omega_R^2 x = 0 \quad \text{and} \quad \ddot{y} + \omega_y^2 y = 0 \quad (2.46)$$

1475 A restoring force (linear terms in  $x$  and  $y$ , Eq. 2.46) arises from the radially varying  
1476 field, characterized by a field index

$$k = \frac{R_0}{B_0} \left. \frac{\partial B_y}{\partial R} \right|_{R=R_0, y=0} \quad (2.47)$$

1477 *Radial stability*: radially this force adds to the geometrical focusing (curvature term  
1478 “1” in  $\omega_R^2$ , Eq. 2.45, Fig. 2.10). In the weakly decreasing field  $B(R)$  an ion with mo-  
1479 mentum  $p = mv$  moving in the vicinity of the  $R_0$ -radius reference orbit experiences  
1480 in the moving frame a resultant force  $F_t = -qvB + m \frac{v^2}{r}$  (Fig. 2.11) of which the  
1481 (outward) component  $f_c = m \frac{v^2}{r}$  decreases with  $r$  at a higher rate than the decrease  
1482 of the Laplace (inward) component  $f_B = -qvB(r)$ . In other words, radial stability  
1483 requires  $BR$  to increase with  $R$ ,  $\frac{\partial BR}{\partial R} = B + R \frac{\partial B}{\partial R} > 0$ , this holds in particular at  $R_0$ ,  
1484 thus  $1 + k > 0$ .

1485 *Axial stability* requires a restoring force directed toward the median plane. Refer-  
1486 ring to Fig. 2.9, this means  $F_y = -a \times y$  (with  $a$  a positive quantity) and thus  $B_R < 0$ ,  
1487 at all  $(r, y \neq 0)$ . This is achieved by designing a guiding field which decreases with  
1488 radius,  $\frac{\partial B_R}{\partial y} < 0$ . Referring to Eq. 2.47 this means  $k < 0$ .

1489 From these radial and axial constraints the condition of “weak focusing” for  
1490 transverse motion stability around the circular equilibrium orbit results, namely,

$$-1 < k < 0 \quad (2.48)$$

1491 Note regarding the geometrical focusing: the focal distance associated with the  
1492 curvature of a magnet of arc length  $\mathcal{L}$  is obtained by integrating  $\frac{d^2 x}{ds^2} + \frac{1}{R_0^2} x = 0$  and  
1493 identifying with the focusing property  $\Delta x' = -x/f$ , namely,

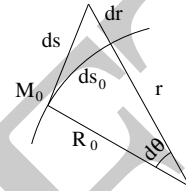
$$\Delta x' = \int \frac{d^2 x}{ds^2} ds \approx \frac{-x}{R^2} \int ds = \frac{-x \mathcal{L}}{R^2}, \text{ thus } f = \frac{R^2}{\mathcal{L}} \quad (2.49)$$

1494 *Isochronism*: the axial focusing constraint,  $B$  decreasing with  $R$ , contributes break-  
 1495 ing the isochronism (in addition to the effect of the mass increase) by virtue of  
 1496  $\omega_{\text{rev}} \propto B$ .

#### 1497 Paraxial Transverse Coordinates

1498 Introduce the path variable  $s$  as the independent variable in Eq. 2.46 and neglect the  
 1499 transverse velocity components ( $1 + \frac{x}{R_0} \approx 1$ ,  $y \ll 0$ ) so that

$$ds = [r^2(s)d\theta^2 + dr^2 + dy^2]^{1/2} \approx |\mathbf{v}|dt \quad (2.50)$$



1500 thus the equations of motion in the moving frame (Eq. 2.46) take the form

$$\frac{d^2 x}{ds^2} + \frac{1+k}{R_0^2} x = 0 \quad \text{and} \quad \frac{d^2 y}{ds^2} - \frac{k}{R_0^2} y = 0 \quad (2.51)$$

1501 Given  $-1 < k < 0$  the motion is that of a harmonic oscillator, in both planes, with  
 1502 respective restoring constants  $(1+k)/R_0^2$  and  $-k/R_0^2$ , both positive quantities. The  
 1503 solution is a sinusoidal motion,

$$\begin{cases} r(s) - R_0 = x(s) = x_0 \cos \frac{\sqrt{1+k}}{R_0}(s - s_0) + x'_0 \frac{R_0}{\sqrt{1+k}} \sin \frac{\sqrt{1+k}}{R_0}(s - s_0) \\ r'(s) = x'(s) = -x_0 \frac{\sqrt{1+k}}{R_0} \sin \frac{\sqrt{1+k}}{R_0}(s - s_0) + x'_0 \cos \frac{\sqrt{1+k}}{R_0}(s - s_0) \end{cases} \quad (2.52)$$

$$\begin{cases} y(s) = y_0 \cos \frac{\sqrt{-k}}{R_0}(s - s_0) + y'_0 \frac{R_0}{\sqrt{-k}} \sin \frac{\sqrt{-k}}{R_0}(s - s_0) \\ y'(s) = -y_0 \frac{\sqrt{-k}}{R_0} \sin \frac{\sqrt{-k}}{R_0}(s - s_0) + y'_0 \cos \frac{\sqrt{-k}}{R_0}(s - s_0) \end{cases} \quad (2.53)$$

1505 Radial and axial wave numbers can be introduced,

$$\nu_R = \frac{\omega_R}{\omega_{\text{rev}}} = \sqrt{1+k} \quad \text{and} \quad \nu_y = \frac{\omega_y}{\omega_{\text{rev}}} = \sqrt{-k} \quad (2.54)$$

1506 *i.e.*, the number of sinusoidal oscillations of the paraxial motion about the reference  
 1507 circular orbit over a turn, respectively radial and axial. Both are less than 1: there  
 1508 is less than one sinusoidal oscillation in a revolution. In addition, as a result of the  
 1509 revolution symmetry of the field,

$$\nu_R^2 + \nu_y^2 = 1 \quad (2.55)$$

1510 *Off-Momentum Orbit*

In a structure with revolution symmetry, the equilibrium trajectory at momentum  $\begin{cases} p_0 \\ p = p_0 + \Delta p \end{cases}$  is at radius  $\begin{cases} R_0 \text{ with } B_0 R_0 = \frac{p_0}{q} \\ R \text{ with } BR = \frac{p}{q} \end{cases}$ , where  $\begin{cases} B = B_0 + \left(\frac{\partial B}{\partial x}\right)_0 \Delta x + \dots \\ R = R_0 + \Delta x \end{cases}$   
 On the other hand

$$BR = \frac{p}{q} \Rightarrow \left[ B_0 + \left(\frac{\partial B}{\partial x}\right)_0 \Delta x + \dots \right] (R_0 + \Delta x) = \frac{p_0 + \Delta p}{q}$$

1511 which, neglecting terms in  $(\Delta x)^2$ , and given  $B_0 R_0 = \frac{p_0}{q}$ , leaves  $\Delta x \left[ \left(\frac{\partial B}{\partial x}\right)_0 R_0 + B_0 \right] = \frac{\Delta p}{q}$ . With  $k = \frac{R_0}{B_0} \left(\frac{\partial B}{\partial x}\right)_0$  this yields

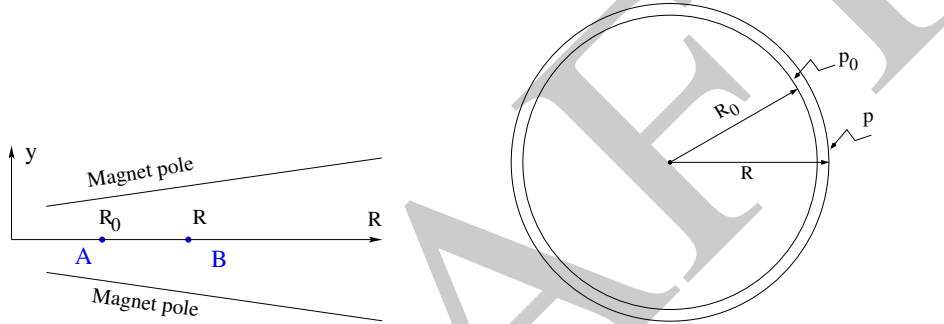


**Fig. 2.12** The equilibrium radius at location A is  $R_0$ , momentum is  $p_0$ , rigidity is  $B_0 R_0$ . The equilibrium radius at B is  $R$ , momentum  $p$ , rigidity  $BR$

1512

$$\Delta x = D \frac{\Delta p}{p_0} \quad \text{with} \quad D = \frac{R_0}{1+k} \quad \text{the dispersion function} \quad (2.56)$$

1513 The dispersion  $D$  is an  $s$ -independent quantity as a result of the revolution symmetry  
 1514 of the field ( $k$  and  $R=p/qB$  are  $s$ -independent).

1515 To the first order in the coordinates, the vertical coordinates  $y(s)$ ,  $y'(s)$  (Eq. 2.53)  
 1516 are unchanged under the effect of a momentum offset, the horizontal trajectory angle  
 1517  $x'(s)$  (Eq. 2.52) is unchanged as well (the circular orbits are concentric, Fig. 2.12)  
 1518 whereas  $x(s)$  satisfies

$$x(s, p_0 + \Delta p) = x(s, p_0) + \Delta p \left. \frac{\partial x}{\partial p} \right|_{s, p_0} = x(s, p_0) + D \frac{\Delta p}{p_0} \quad (2.57)$$

1519 *Orbit and revolution period lengthening*

1520 A  $\delta p$  momentum offset results in (Eq. 2.56)

$$\frac{\delta C}{C} = \frac{\delta R}{R} = \frac{\delta x}{R} = \alpha \frac{\delta p}{p} \quad \text{with} \quad \alpha = \frac{1}{1+k} = \frac{1}{\gamma^2 R} \quad (2.58)$$

1521 with  $\alpha$  the momentum compaction, a positive quantity: orbit length increases with  
 1522 momentum. Substituting  $\frac{\delta \beta}{\beta} = \frac{1}{\gamma^2} \frac{\delta p}{p}$ , the change in revolution period  $T_{\text{rev}} = C/\beta c$   
 1523 with momentum writes

$$\frac{\delta T_{\text{rev}}}{T_{\text{rev}}} = \frac{\delta C}{C} - \frac{\delta \beta}{\beta} = \left( \alpha - \frac{1}{\gamma^2} \right) \frac{\delta p}{p} \quad (2.59)$$

1524 Given that  $-1 < k < 0$  and  $\gamma \gtrsim 1$ , it results that  $\alpha - 1/\gamma^2 > 0$ : the revolution period  
 1525 increases with energy, the increase in radius is faster than the velocity increase.

### 1526 2.2.3 Quasi-Isochronous Resonant Acceleration

1527 The energy  $W$  of an accelerated ion (in the non-relativistic energy domain of the  
 1528 classical cyclotron) satisfies the frequency dependence

$$W = \frac{1}{2} m v^2 = \frac{1}{2} m (2\pi R f_{\text{rev}})^2 = \frac{1}{2} m \left( 2\pi R \frac{f_{\text{rf}}}{h} \right)^2 \quad (2.60)$$

1529 Observe in passing: given the cyclotron size (radius  $R$ ),  $f_{\text{rf}}$  and  $h$  set the limit for  
 1530 the acceleration range. The revolution frequency decreases with energy and the  
 1531 condition of synchronism with the oscillating voltage,  $f_{\text{rf}} = h f_{\text{rev}}$ , is only fulfilled  
 1532 at that particular radius where  $\omega_{\text{rf}} = qB/m$  (Fig. 2.13-left). The out-phasing  $\Delta\phi$  of  
 1533 the RF at ion arrival at the gap builds-up turn after turn, decreasing in a first stage  
 1534 (towards lower voltages in Fig. 2.13-right) and then increasing back to  $\phi = \pi/2$  and  
 1535 beyond towards  $\pi$ . Beyond  $\phi = \pi$  the RF voltage is decelerating.

1536 With  $\omega_{\text{rev}}$  constant between two gap passages, differentiating  $\phi(t)$  (Eq. 2.38)  
 1537 yields  $\dot{\phi} = \omega_{\text{rf}} - \omega_{\text{rev}}$ . Between two gap passages on the other hand,  $\Delta\phi = \dot{\phi}\Delta T =$   
 1538  $\dot{\phi} T_{\text{rev}}/2 = \dot{\phi} \frac{\pi R}{v}$ , yielding a phase-shift of

$$\text{half-turn} \quad \Delta\phi = \pi \left( \frac{\omega_{\text{rf}}}{\omega_{\text{rev}}(R)} - 1 \right) = \pi \left( \frac{m\omega_{\text{rf}}}{qB(R)} - 1 \right) \quad (2.61)$$

1539 The out-phasing is thus a gap-after-gap, cumulative effect. Due to this the classical  
 1540 cyclotron requires quick acceleration (small number of turns), which means high  
 1541 voltage (tens to hundreds of kVolts). As expected, with  $\omega_{\text{rf}}$  and  $B$  constant,  $\phi$  presents  
 1542 a minimum ( $\dot{\phi} = 0$ ) at  $\omega_{\text{rf}} = \omega_{\text{rev}} = qB/m$  where exact isochronism is reached  
 1543 (Fig. 2.13). The upper limit to  $\phi$  is set by the condition  $\Delta W > 0$ : acceleration.

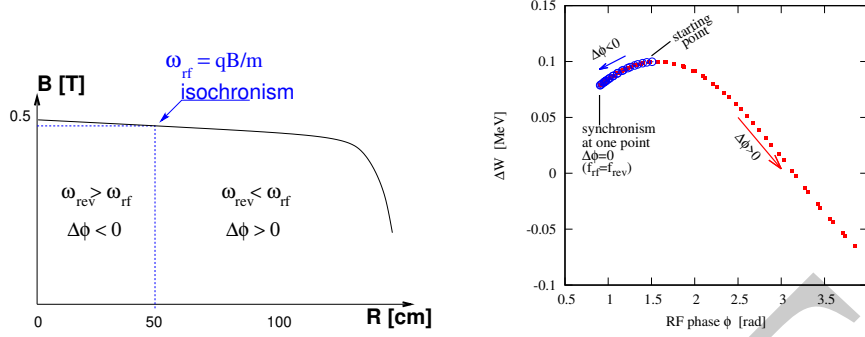
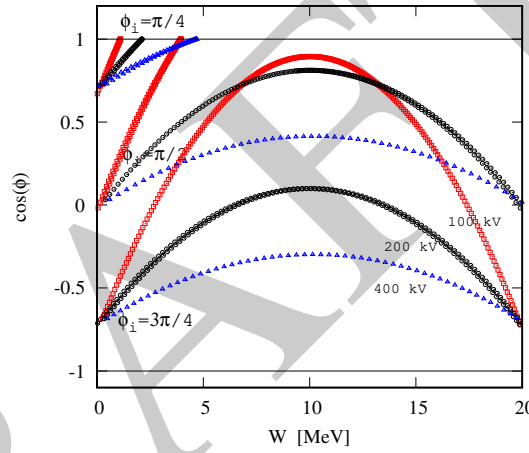


**Fig. 2.13** Left: a sketch of the synchronism condition at one point ( $h=1$  assumed). Right: the span in phase of the energy gain  $\Delta W = q\hat{V} \sin \phi$  (Eq. 2.38) over the acceleration cycle

**Fig. 2.14** A graph of the cyclotron equation (Eq. 2.62), for three different accelerating voltages: 100, 200 and 400 kV/gap (respectively square, circle and triangle markers). The sole settings resulting in  $-1 < \cos \phi(E) < 1$ ,  $\forall E$ , allow complete acceleration to top energy.  $\phi_i = \pi/4$  at injection for instance, does not (upper three curves).  $\phi_i = 3\pi/4$  works (lower three curves), with as low as 100 kV/gap



1544 The cyclotron equation determines the achievable energy range, depending on  
 1545 the injection energy  $E_i$ , the RF phase at injection  $\phi_i$ , the RF frequency  $\omega_{rf}$  and gap  
 1546 voltage  $\hat{V}$ . It writes [12]

$$\cos \phi = \cos \phi_i + \pi \left[ 1 - \frac{\omega_{rf}}{\omega_{rev}} \frac{E + E_i}{2M} \right] \frac{E - E_i}{q\hat{V}} \quad (2.62)$$

1547 Equation 2.62 is represented in Fig. 2.14 for various values of the peak voltage  
 1548 and phase at injection  $\phi_i$ .  $M$  [eV/c<sup>2</sup>] and  $E$  [eV] are respectively the rest mass and  
 1549 relativistic energy,  $q\hat{V}$  is expressed in electron-volts, the index  $i$  denotes injection  
 1550 parameters.

## 1551 2.2.4 Beam Extraction

1552 From  $R = p/qB$  and assuming  $B(R) \approx \text{constant}$  (this is legitimate as  $k$  is normally  
1553 small), in the non-relativistic approximation ( $W \ll M$ ,  $W = p^2/2M$ ) one gets

$$\frac{dR}{R} = \frac{1}{2} \frac{dW}{W} \quad (2.63)$$

1554 Integrating yields

$$R^2 = R_i^2 \frac{W}{W_i} \quad (2.64)$$

1555 with  $R_i, W_i$  initial conditions. From Eqs. 2.63, 2.64, assuming  $W_i \ll W$  and constant  
1556 acceleration rate  $dW$  such that  $W = n dW$  after  $n$  turns, one gets the scaling laws

$$R \propto \sqrt{n}, \quad dR \propto \frac{R}{W} \propto \frac{1}{R} \propto dW, \quad \frac{dR}{dn} = \frac{R}{2n} \quad (2.65)$$

1557 The turn separation  $dR$  is proportional to the energy gain per turn and inversely  
1558 proportional to the orbit radius.

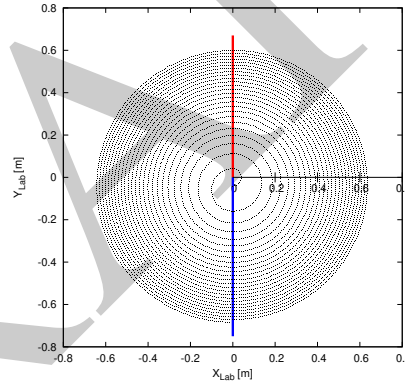


**Fig. 2.15** The radial distance between successive turns decreases with energy, in inverse proportion to the orbit radius. The red and blue segments here figure the accelerating gap

1559 The radial distance between successive turns decreases with energy, toward zero  
1560 (Fig. 2.15), eventually resulting in insufficient spacing for insertion of an extraction  
1561 septum.

### 1562 *Orbit modulation*

1563 Consider an ion bunch injected in the cyclotron with some  $(x_0, x'_0)$  conditions in  
1564 the vicinity of the reference orbit, and assume slow acceleration. While accelerated  
1565 the bunch undergoes an oscillatory motion around the equilibrium orbit (Eq. 2.52).  
1566 Observed at the extraction septum this oscillation modulates the distance of the



1567 bunch to the local equilibrium orbit, moving it outwards or inwards depending on  
 1568 the turn number, which modulates the distance between the accelerated turns. This  
 1569 effect can be resorted to, so to increase the separation between the final two turns  
 1570 and so enhance the extraction efficiency [9].

### 1571 2.2.5 Spin Dance

1572 “Much of the physics of spin motion can be illustrated using the simplest model of a  
 1573 storage ring consisting of uniform horizontal bending and no straight sections.” [13].

1574 By virtue of this statement, a preliminary introduction to spin motion in magnetic  
 1575 fields is given in the present chapter. In support to this in addition, comes the fact that  
 1576 cyclotrons happened to be the first circular machines to accelerate polarized beams  
 1577 (first acceleration of polarized beams had happened earlier in the 1960s, using  
 1578 electrostatic columns at voltage generators, when polarized proton and deuteron  
 1579 sources began operating [14]).

1580 The magnetic field  $\mathbf{B}$  of the cyclotron dipole exerts a torque on the spin angular  
 1581 momentum  $\mathbf{S}$  of an ion, causing it to precess following the Thomas-BMT differential  
 1582 equation [15]

$$\frac{d\mathbf{S}}{dt} = \mathbf{S} \times \underbrace{\frac{q}{m} [(1+G)\mathbf{B}_{\parallel} + (1+G\gamma)\mathbf{B}_{\perp}]}_{\omega_{\text{sp}}} \quad (2.66)$$

1583 where  $t$  is the time;  $\omega_{\text{sp}}$  the precession vector: a combination of  $\mathbf{B}_{\parallel}$  and  $\mathbf{B}_{\perp}$  compo-  
 1584 nents of  $\mathbf{B}$  respectively parallel and orthogonal to the ion velocity vector.  $G$  is the  
 1585 gyromagnetic anomaly,

1586  $G=1.7928474$  (proton),  $-0.178$  (Li),  $-0.143$  (deuteron),  $-4.184$  ( $^3\text{He}$ ) ...

1587  $\mathbf{S}$  in this equation is in the ion rest frame, all other quantities are in the laboratory  
 1588 frame.

1589 In the case of an ion moving in the median plane of the dipole,  $\mathbf{B}_{\parallel} = 0$ , thus the  
 1590 precession axis is parallel to the magnetic field vector,  $\mathbf{B}_y$ , so that  $\omega_{\text{sp}} = \frac{q}{m} (1 +$   
 1591  $G\gamma)\mathbf{B}_y$ . The spin precession angle over a trajectory arc  $\mathcal{L}$  is

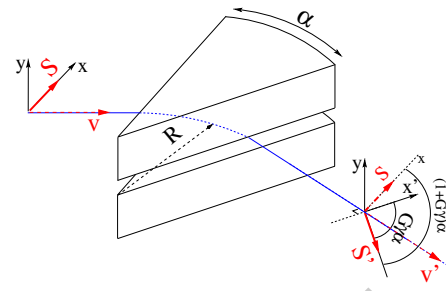
$$\theta_{\text{sp, Lab}} = \frac{1}{v} \int_{(\mathcal{L})} \omega_{\text{sp}} ds = (1+G\gamma) \frac{\int_{(\mathcal{L})} B ds}{BR} = (1+G\gamma)\alpha \quad (2.67)$$

1592 with  $\alpha$  the velocity vector precession (Fig. 2.16). The precession angle in the moving  
 1593 frame (the latter rotates by an angle  $\alpha$  along  $\mathcal{L}$ ) is

$$\theta_{\text{sp}} = G\gamma\alpha \quad (2.68)$$

1594 thus the number of  $2\pi$  spin precessions per ion orbit around the cyclotron is  $G\gamma$ . By  
 1595 analogy with the wave numbers (Eq. 2.54) this defines the “spin tune”

**Fig. 2.16** Spin and velocity vector precession in a constant field, from  $\mathbf{S}$  to  $\mathbf{S}'$  and  $\mathbf{v}$  to  $\mathbf{v}'$  respectively. In the moving frame the spin precession along the arc  $\mathcal{L} = R\alpha$  is  $G\gamma\alpha$ , in the laboratory frame the spin precesses by  $(1 + G\gamma)\alpha$



$$v_{\text{sp}} = G\gamma \quad (2.69)$$

DRAFT

## 1596 2.3 Exercises

1597 Note: some of the input data files for these simulations are available in zgoubi  
 1598 sourceforge repository at  
 1599 [https://sourceforge.net/p/zgoubi/code/HEAD/tree/branches/exemples/book/zgoubiMaterial/cyclotron\\_classical/](https://sourceforge.net/p/zgoubi/code/HEAD/tree/branches/exemples/book/zgoubiMaterial/cyclotron_classical/)

### 1600 2.5 Modeling a Cyclotron Dipole: Using a Field Map

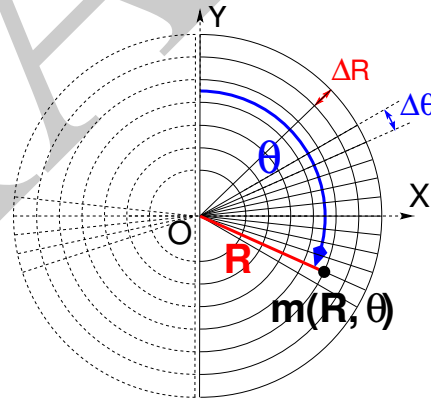
1601 Solution: page 315

1602 In this exercise, ion trajectories are ray-traced, various optical properties addressed  
 1603 in the foregoing are recovered, using a field map to simulate the cyclotron dipole.  
 1604 Fabricating that field map is a preliminary step of the exercise.

1605 The interest of using a field map is that it is an easy way to account for fancy  
 1606 magnet geometries and fields, including field gradients and possible defects. A  
 1607 field map can be generated using mathematical field models, or from magnet com-  
 1608 putation codes, or from magnetic measurements. The first method is used, here.  
 1609 TOSCA[MOD.MOD1=22.1] keyword [16, cf. INDEX] is used to ray-trace through  
 1610 the map.

1611 *Working hypotheses:* A 2-dimensional  $m(R, \theta)$  polar meshing of the median plane  
 1612 is considered (Fig. 2.17). It is defined in a  $(O; X, Y)$  frame and covers an angular  
 1613 sector of a few tens of degrees. The mid-plane field map is the set of values  $B_z(R, \theta)$   
 1614 at the nodes of the mesh. During ray-tracing, TOSCA[MOD.MOD1=22.1] extrapolates  
 1615 the field along 3D space  $(R, \theta, Z)$  ion trajectories from the 2D polar map [16].

**Fig. 2.17** Principle of a 2D field map in polar coordinates, covering a  $180^\circ$  sector (over the right hand side dee). The mesh nodes  $m(R, \theta)$  are distant  $\Delta R$  radially,  $\Delta\theta$  azimuthally. The map is used twice to cover the  $360^\circ$  cyclotron dipole as sketched here, while allowing insertion of an accelerating gap between the two dees



1616 (a) Construct a  $180^\circ$  two-dimensional map of a median plane field  $B_z(R, \theta)$ ,  
 1617 proper to simulate the field in a cyclotron as sketched in Fig. 2.1. Use one of  
 1618 the following two methods: either (i) write an independent program, or (ii) use  
 1619 zgoubi and its analytical field model DIPOLE, together with the keyword OP-  
 1620 TIONS[CONSTY=ON] [16, cf. INDEX].

1621 Besides: use a uniform mesh (Fig. 2.17) covering from  $R_{\min}=1$  to  $R_{\max}=76$  cm,  
 1622 with radial increment  $\Delta R = 0.5$  cm, azimuthal increment  $\Delta\theta = 0.5$  [cm]/ $R_0$  with  $R_0$

1623 some reference radius (say, 50 cm, in view of subsequent exercises), and constant  
 1624 axial field  $B_Z = 5$  kG. The appropriate 6-column formatting of the field map data  
 1625 for TOSCA[MOD.MOD1=22.1] to read is the following:

1626  $R \cos \theta, Z, R \sin \theta, BY, BZ, BX$

1627 with  $\theta$  varying first,  $R$  varying second;  $Z$  is the vertical direction (normal to the map  
 1628 mesh),  $Z \equiv 0$  in the present case. Note that proper functioning of TOSCA requires  
 1629 the field map to begin with the following line of numerical values:

1630 Rmin [cm]  $\Delta R$  [cm]  $\Delta \theta$  [deg]  $Z$  [cm]

1631 Produce a graph of the  $B_Z(R, \theta)$  field map content.

1632 (b) Ray-trace a few concentric circular mid-plane trajectories centered on the  
 1633 center of the dipole, ranging in  $10 \leq R \leq 80$  cm. Produce a graph of these concentric  
 1634 trajectories in the  $(O; X, Y)$  laboratory frame.

1635 Initial coordinates can be defined using OBJET, particle coordinates along tra-  
 1636 jectories during the stepwise ray-tracing can be logged in zgoubi.plt by setting IL=2  
 1637 under TOSCA. In order to find the Larmor radius corresponding to a particular  
 1638 momentum, the matching procedure FIT can be used. In order to repeat the latter for  
 1639 a series of different momenta, REBELOTE[IOPT=1] can be used.

1640 Explain why it is possible to push the ray-tracing beyond the 76 cm radial extent  
 1641 of the field map.

1642 (c) Compute the orbit radius  $R$  and the revolution period  $T_{\text{rev}}$  as a function of  
 1643 kinetic energy  $W$  or rigidity  $BR$ . Produce a graph, including for comparison the  
 1644 theoretical dependence of  $T_{\text{rev}}$ .

1645 (d) Check the effect of the density of the mesh (the choice of  $\Delta R$  and  $\Delta \theta$  values,  
 1646 *i.e.*, the number of nodes  $N_\theta \times N_R = (1 + \frac{180^\circ}{\Delta \theta}) \times (1 + \frac{80 \text{ cm}}{\Delta R})$ ), on the accuracy of the  
 1647 trajectory and time-of-flight computation.

1648 (e) Check the effect of the integration step size on the accuracy of the trajectory  
 1649 and time-of-flight computation, by considering a small  $\Delta s = 1$  cm and a large  
 1650  $\Delta s = 10$  cm, at 200 keV and 5 MeV (proton), and comparing with theory.

1651 (f) Consider a periodic orbit, thus its radius  $R$  should remain unchanged after  
 1652 stepwise integration of the motion over a turn. However, the size  $\Delta s$  of the numerical  
 1653 integration step has an effect on the final value of the radius:

1654 For two different cases, 200 keV (a small orbit) and 5 MeV (a larger one), provide a  
 1655 graph of the dependence of the relative error  $\delta R/R$  after one turn, on the integration  
 1656 step size  $\Delta s$  (consider a series of  $\Delta s$  values in a range  $\Delta s : 0.1 \text{ mm} \rightarrow 20 \text{ cm}$ ).  
 1657 REBELOTE[IOPT=1] do-loop can be used to repeat the one-turn raytracing with  
 1658 different  $\Delta s$ .

## 1659 2.6 Modeling a Cyclotron Dipole: Using an Analytical Field Model

1660 Solution: page 323

1661 This exercise is similar to exercise 2.5, yet using the analytical modeling DIPOLE,  
 1662 instead of a field map. DIPOLE provides the  $Z$ -parallel median plane field  $\mathbf{B}(R, \theta, Z =$   
 1663  $0) \equiv \mathbf{B}_Z(R, \theta, Z = 0)$  at the projected  $m(R, \theta, Z = 0)$  ion location (Fig. 2.18), while  
 1664  $\mathbf{B}(R, \theta, Z)$  at particle location is obtained by extrapolation.

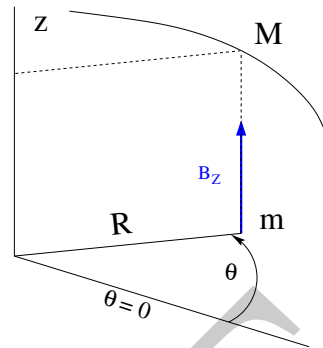


**Fig. 2.18** DIPOLE provides the value  $B_z(m)$  of the median plane field at  $m$ , projection of particle position  $M(R, \theta, Z)$  in the median plane.  $\mathbf{B}(R, \theta, Z)$  is obtained by extrapolation

1665 (a) Simulate a  $180^\circ$  sector dipole; DIPOLE requires a reference radius [16,  
1666 Eqs. 6.3.19-21], noted  $R_0$  here; for the sake of consistency with other exercises, it is  
1667 suggested to take  $R_0 = 50$  cm. Take a constant axial field  $B_z = 5$  kG.

1668 Explain the various data that define the field simulation in DIPOLE: geometry,  
1669 role of  $R_0$ , field and field indices, fringe fields, integration step size, etc.

1670 Produce a graph of  $B_z(R, \theta)$ .

1671 (b) Repeat question (b) of exercise 2.5.

1672 (c) Repeat question (c) of exercise 2.5.

1673 (d) As in question (e) of exercise 2.5, check the effect of the integration step size  
1674 on the accuracy of the trajectory and time-of-flight computation.

1675 Repeat question (f) of exercise 2.5.

1676 (e) From the two series of results (exercise 2.5 and the present one), comment on  
1677 various pros and cons of the two methods, field map versus analytical field model.

## 1678 2.7 Resonant Acceleration

1679 Solution: page 327

1680 Based on the earlier exercises, using indifferently a field map (TOSCA) or an  
1681 analytical model of the field (DIPOLE), introduce a sinusoidal voltage between the  
1682 two dees, with peak value 100 kV. Assume that ion motion does not depend on RF  
1683 phase: the boost through the gap is the same at all passes, use CAVITE[IOPT=3] [16,  
1684 cf. INDEX] for that. Note that using CAVITE requires prior PARTICUL in order to  
1685 specify ion species and data, necessary to compute the energy boost (Eq. 2.38).

1686 (a) Accelerate a proton with initial kinetic energy 20 keV, up to 5 MeV, take  
1687 harmonic  $h=1$ . Produce a graph of the accelerated trajectory in the laboratory frame.

1688 (b) Provide a graph of the proton momentum  $p$  and total energy  $E$  as a function  
1689 of its kinetic energy, both from this numerical experiment (ray-tracing data can be  
1690 stored using FAISTORE) and from theory, all on the same graph.

1691 (c) Provide a graph of the normalized velocity  $\beta = v/c$  as a function of kinetic  
1692 energy, both numerical and theoretical, and in the latter case both classical and  
1693 relativistic.

1694 (d) Provide a graph of the relative change in velocity  $\Delta\beta/\beta$  and orbit length  $\Delta C/C$   
 1695 as a function of kinetic energy, both numerical and theoretical. From their evolution,  
 1696 conclude that the time of flight increases with energy.

1697 (e) Repeat the previous questions, assuming a harmonic  $h=3$  RF frequency.

## 1698 2.8 Spin Dance

1699 Solution: page 331

1700 Cyclotron modeling in the present exercise can use Exercise 2.5 or Exercise 2.6  
 1701 technique (*i.e.*, a field map or an analytical field model), indifferently.

1702 (a) Add spin transport, using SPNTRK [16, *cf.* INDEX]. Produce a listing  
 1703 (zgoubi.res) of a simulation, including spin outcomes.

1704 Note: PARTICUL is necessary here, for the spin equation of motion (Eq. 2.66) to  
 1705 be solved [16, Sect. 2]. SPNPRT can be used to have local spin coordinates listed in  
 1706 zgoubi.res (at the manner that FAISCEAU lists local particle coordinates).

1707 (b) Consider proton case, take initial spin longitudinal, compute the spin preces-  
 1708 sion over one revolution, as a function of energy over a range 12 keV  $\rightarrow$  5 MeV. Give  
 1709 a graphical comparison with theory.

1710 FAISTORE can be used to store local particle data, which include spin coord-  
 1711 inates, in a zgoubi.fai style output file. IL=2 [16, *cf.* INDEX] (under DIPOLE or  
 1712 TOSCA, whichever modeling is used) can be used to obtain a print out of particle  
 1713 and spin motion data to zgoubi.plt during stepwise integration.

1714 (c) Inject a proton with longitudinal initial spin  $S_i$ . Give a graphic of the lon-  
 1715 gitudinal spin component value as a function of azimuthal angle, over a few turns  
 1716 around the ring. Deduce the spin tune from this computation. Repeat for a couple of  
 1717 different energies.

1718 Place both FAISCEAU and SPNPRT commands right after the first dipole sector,  
 1719 and use them to check the spin rotation and its relationship to particle rotation, right  
 1720 after the first passage through that first sector.

1721 (d) Spin dance: the input data file optical sequence here is assumed to model a  
 1722 full turn. Inject an initial spin at an angle from the horizontal plane (this is in order  
 1723 to have a non-zero vertical component), produce a 3-D animation of the spin dance  
 1724 around the ring, over a few turns.

1725 (e) Repeat questions (b-d) for two additional ions: deuteron (much slower spin  
 1726 precession),  ${}^3\text{He}^{2+}$  (much faster spin precession).

## 1727 2.9 Synchronized Spin Torque

1728 Solution: page 337

1729 A synchronized spin kick is superimposed on orbital motion. An input data file for  
 1730 a complete cyclotron is considered as in question 2.8 (d), for instance six 60 degree  
 1731 DIPOLES, or two 180 degree DIPOLES.

1732 Insert a local spin rotation of a few degrees around the longitudinal axis, at the  
 1733 end of the optical sequence (*i.e.*, after one orbit around the cyclotron). SPINR can be  
 1734 used for that, rather than a local magnetic field, so to avoid any orbital effect. Track  
 1735 4 particles on their respective equilibrium orbit, with energies 0.2, 108.412, 118.878  
 1736 and 160.746 MeV.

1737 Produce a graph of the motion of the vertical spin component  $S_y$  along the circular  
1738 orbit.

1739 Produce a graph of the spin vector motion on a sphere.

### 1740 2.10 Weak Focusing

1741 Solution: page 340

1742 (a) Consider a  $60^\circ$  sector as in earlier exercises (building a field map and using  
1743 TOSCA as in exercise 2.5, or using DIPOLE as in exercise 2.6), construct the sector  
1744 accounting for a non-zero radial index  $k$  in order to introduce axial focusing, say  
1745  $k = -0.03$ , assume a reference radius  $R_0$  for a reference energy of 200 keV ( $R_0$  and  
1746  $B_0$  are required in order to define the index  $k$ , Eq. 2.47). Ray-trace that 200 keV  
1747 reference orbit, plot it in the lab frame: make sure it comes out as expected, namely,  
1748 constant radius, final and initial angles zero.

1749 (b) Using FIT[2], find and plot the radius dependence of orbit rigidity,  $BR(R)$ ,  
1750 from ray-tracing over a  $BR$  range covering 20 keV to 5 MeV; superpose the theoretical  
1751 curve. REBELOTE[IOPT=1] can be used to perform the scan.

1752 (c) Produce a graph of the paraxial axial motion of a 1 MeV proton, over a few  
1753 turns (use IL=2 under TOSCA, or DIPOLE, to have step by step particle and field  
1754 data logged in zgoubi.plt). Check the effect of the focusing strength by comparing  
1755 the trajectories for a few different index values, including close to -1 and close to 0.

1756 (d) Produce a graph of the magnetic field experienced by the ion along these  
1757 trajectories.

### 1758 2.11 Loss of Isochronism

1759 Solution: page 349

1760 Compare on a common graphic the revolution period  $T_{\text{rev}}(R)$  for a field index  
1761 value  $k \approx -0.95, -0.5, -0.03, 0^-$ . The scan method of exercise 2.10, based on  
1762 REBELOTE[IOPT=1] preceded by FIT[2], can be referred to.

### 1763 2.12 Ion Trajectories

1764 Solution: page 351

1765 In this exercise individual ion trajectories are computed. DIPOLE or TOSCA  
1766 magnetic field modeling can be used, indifferently. No acceleration here, ions circle  
1767 around the cyclotron at constant energy.

1768 (a) Produce a graph of the horizontal  $x(s)$  and vertical  $y(s)$  trajectory coordinates  
1769 of an ion with rigidity close to  $BR(R_0)$  ( $R_0$  is the reference radius in the definition of  
1770 the index  $k$ ), over a few turns around the cyclotron. From the number of turns, give  
1771 an estimate of the wave numbers. Check the agreement with the expected  $\nu_R(k)$ ,  
1772  $\nu_y(k)$  values (Eq. 2.54).

1773 (b) Consider now protons at 1 MeV and 5 MeV, far from the reference energy  
1774  $E(R_0)$ ; the wave numbers change with energy: consistency with theory can be  
1775 checked. Find their theoretical values, compare with numerical outcomes.

1776 (c) Consider proton, 200 keV energy, plot as a function of  $s$  the difference between  
1777  $x(s)$  from raytracing and its values from Eq. 2.52. Same for  $y(s)$  compared to Eq. 2.53.

1778 IL=2 can be used to store in zgoubi.plt the step-by-step particle coordinates across  
1779 DIPOLE.

1780 (d) Perform a scan of the wave numbers over 200 keV–5 MeV energy inter-  
1781 val, computed using OBJET[KOBJ=5] and MATRIX[IORD=1,IFOC=11], or OB-  
1782 JET[KOBJ=6] and MATRIX[IORD=2,IFOC=11], together with REBELOTE[IOPT=1]  
1783 to repeat MATRIX for a series of energy values.

### 1784 2.13 RF Phase at the Accelerating Gap

1785 Solution: page 357

1786 Consider the cyclotron model of exercise 2.10: field index  $k = -0.03$  defined at  
1787  $R_0 = 50$  cm, field  $B_0 = 5$  kG on that radius. two dees, double accelerating gap.

1788 Accelerate a proton from 1 to 5 MeV: get the turn-by-turn phase-shift at the gaps;  
1789 use CAVITE[IOPT=7] to simulate the acceleration. Compare the half-turn  $\Delta\phi$  so  
1790 obtained with the theoretical expectation (Eq. 2.61). Produce similar graphs  $B(R)$   
1791 and  $\Delta W(\phi)$  to Fig. 2.13.

1792 Accelerate over more turns, observe the particle decelerating.

### 1793 2.14 The Cyclotron Equation

1794 Solution: page 359

1795 The cyclotron model of exercise 2.7 is considered: two dees, double accelerating  
1796 gap, uniform field  $B = 5$  kG, no field gradient needed here (no vertical motion).

1797 (a) Set up an input data file for the simulation of a proton acceleration from  
1798 0.2 to 20 MeV. In particular, assume that  $\cos(\phi)$  reaches its maximum value at  
1799  $W_m = 10$  MeV; find the RF voltage frequency from  $d(\cos \phi)/dW = 0$  at  $W_m$ .

1800 (b) Give a graph of the energy-phase relationship (Eq. 2.62), for  $\phi_i = \frac{3\pi}{4}, \frac{\pi}{2}, \frac{\pi}{4}$ ,  
1801 from both simulation and theory.

### 1802 2.15 Cyclotron Extraction

1803 Solution: page 361

1804 (a) Acceleration of a proton in a uniform field  $B = 5$  kG is first considered (field  
1805 hypotheses as in exercise 2.7). RF phase is ignored: CAVITE[IOPT=3] can be used  
1806 for acceleration. Take a 100 kV gap voltage.

1807 Compute the distance  $\Delta R$  between turns, as a function of turn number and of  
1808 energy, over the range  $E : 0.02 \rightarrow 5$  MeV. Compare graphically with theoretical  
1809 expectation.

1810 (b) Assume a beam with Gaussian momentum distribution and *rms* momentum  
1811 spread  $\delta p/p = 10^{-3}$ . An extraction septum is placed half-way between two successive  
1812 turns, provide a graph of the percentage of beam loss at extraction, as a function of  
1813 extraction turn number. COLLIMA can be used for that simulation and for particle  
1814 counts, it also allows for possible septum thickness.

1815 (c) Repeat (a) and (b) considering a field with index: take for instance  $B_0 = 5$  kG  
1816 and  $k = -0.03$  at  $R_0 = R(0.2 \text{ MeV}) = 12.924888$  cm.

1817 (d) Investigate the effect of injection conditions ( $Y_i, T_i$ ) on the modulation of the  
1818 distance between turns.



1819 Try and confirm numerically that, with slow acceleration, the oscillation is mini-  
 1820 mized for an initial  $|T_i| = \left| \frac{x_0 v_R}{R} \right|$  (after Ref. [9, p. 133]).

## 1821 2.16 Acceleration and Extraction of a 6-D Polarized Bunch

1822 Solution: page 366

1823 The cyclotron simulation hypotheses of exercise 2.14-a are considered; account  
 1824 or  $k = -0.02$  field index.

1825 Add a short “high energy” extraction line, say 1 meter, following REBELOTE in  
 1826 the optical sequence, ending up with a “Beam\_Dump” MARKER for instance.

1827 (a) Create a 1,000 ion bunch with the following initial parameters:

1828 - random Gaussian transverse phase space densities, centered on the equilibrium  
 1829 orbit, truncated at 3 sigma, normalized *rms* emittances  $\varepsilon_Y = \varepsilon_Z = 1 \pi \mu\text{m}$ , both  
 1830 emittances matched to the 0.2 MeV orbit optics,

1831 - uniform bunch momentum density  $0.2 \times (1 - 10^{-3}) \leq p \leq 0.2 \times (1 + 10^{-3})$  MeV,  
 1832 matched to the dispersion, namely (Eq. 2.57),  $\Delta x = D \frac{\Delta p}{p}$ ,

1833 - random uniform longitudinal distribution  $-0.5 \leq s \leq 0.5$  mm,

1834 Note: two ways to create this object are, (i) using MCOBJET[KOBJ=3] which  
 1835 generates a random distribution, or (ii) using OBJET[KOBJ=3] to read an external  
 1836 particle coordinate file.

1837 Add spin tracking request (SPNTRK), all initial spins normal to the bend plane.

1838 Produce a graph of the three initial 2-D phase spaces: (Y,T), (Z,P), ( $\delta l, \delta p/p$ ),  
 1839 matched to the 200 keV periodic optics. Provide Y, Z, dp/p,  $\delta l$  and  $S_Z$  histograms  
 1840 (HISTO can be used), check the distribution parameters.

1841 (b) Accelerate this polarized bunch to 20 MeV, using the following RF conditions:

1842 - 200 kV peak voltage,

1843 - RF harmonic 1,

1844 - initial RF phase  $\phi_i = \pi/4$ .

1845 Produce a graph of the three phase spaces as observed downstream of the extrac-  
 1846 tion line. Provide the Y, Z, dp/p,  $\delta l$  and  $S_Z$  histograms. Compare the distribution  
 1847 parameters with the initial values.

1848 What causes the spins to spread away from vertical?

## 1849 References

- 1850 1. Sessler, A., Wilson, E.: Engines of Discovery. A century of particle accelerators. World  
 1851 Scientific (2007)
- 1852 2. Lawrence, E.O., Livingston, M.S. Phys. Rev. 37, 1707 (1931), 1707; Phys. Rev. 38, 136,  
 1853 (1931); Phys. Rev. 40, 19 (1932)
- 1854 3. Credit: Lawrence Berkeley National Laboratory. ©The Regents of the University of California,  
 1855 Lawrence Berkeley National Laboratory
- 1856 4. Lawrence, E.O. and Livingston, M.S.: The Production of High Speed Light Ions Without the  
 1857 Use of High Voltages. Phys. Rev. 40, 19-35 (1932)
- 1858 5. Livingston, M.S., McMillan, E.M.: History of the cyclotron. Physics Today, 12(10) (1959).  
 1859 <https://escholarship.org/uc/item/29c6p35w>

- 1860 6. Bethe, H. E., Rose, M. E.: Maximum energy obtainable from cyclotron. Phys. Rev. 52 (1937)  
1861 1254
- 1862 7. Cole, F.T.: O Camelot ! A memoir of the MURA years (April 1, 1994).  
1863 <https://accelconf.web.cern.ch/c01/cyc2001/extra/Cole.pdf>
- 1864 8. Thomas, L.H.: The Paths of Ions in the Cyclotron. Phys. Rev. 54, 580, (1938).  
1865 Craddock, M.K.: AG focusing in the Thomas cyclotron of 1938. Proceedings of PAC09,  
1866 Vancouver, BC, Canada, FR5REP1
- 1867 9. Stambach, T.: Introduction to Cyclotrons. CERN accelerator school, cyclotrons, linacs and  
1868 their applications. IBM International Education Centre, La Hulpe, Belgium, 28 April-5 May  
1869 1994.  
1870 Fig. 2.4: Stambach, T.: Introduction to Cyclotrons. CERN Yellow Re-  
1871 port 96-02 (1996), Figure 8, page 15. Copyright/License CERN CC-BY-3.0  
1872 <https://creativecommons.org/licenses/by/3.0>, no change to the material
- 1873 10. Baron, E., et al.: The GANIL Injector. Proceedings of the 7th International Conference on  
1874 Cyclotrons and their Applications, Zürich, Switzerland (1975).  
1875 <http://accelconf.web.cern.ch/c75/papers/b-05.pdf>
- 1876 11. Cohen, L.B.: Cyclotrons and Synchrocyclotrons. In Encyclopedia of Physics, Vol. XLIV,  
1877 Nuclear Instrumentation I. Editor S. Flügge. Springer-Verlag, 1959
- 1878 12. Le Duff, J.: Longitudinal beam dynamics in circular accelerators. CERN Accelerator School,  
1879 Jyväskylä, Finland, 7-18 September 1992
- 1880 13. Montague, B.W.: Polarized beams in high energy storage rings. Phys. Rep. (Rev. Sect. Phys.  
1881 Lett.) 113(1), 1-96 (1984)
- 1882 14. Thomas Roser, Anatoli Zelensky, private communication, BNL, June 2021.  
1883 Günther Clausnitzer: History of Polarized Ion Source Developments. In: International Work-  
1884 shop on Polarized Ion Sources and Polarized Gas Jets, February 12-17, 1990, KEK, Tsukuba,  
1885 Japan. KEK Report 90-15, November 1990, edited by Y. MORI.  
1886 [https://inis.iaea.org/collection/NCLCollectionStore/\\_Public/22/051/22051667.pdf](https://inis.iaea.org/collection/NCLCollectionStore/_Public/22/051/22051667.pdf)
- 1887 15. Méot, F.: Spin Dynamics. In: Polarized Beam Dynamics and Instrumentation in Particle  
1888 Accelerators, USPAS Summer 2021 Spin Class Lectures, Springer Nature, Open Access  
1889 (2023).  
1890 <https://link.springer.com/book/10.1007/978-3-031-16715-7>
- 1891 16. Méot, F.: Zgoubi Users' Guide. <https://www.osti.gov/biblio/1062013-zgoubi-users-guide>.  
1892 Sourceforge latest version: <https://sourceforge.net/p/zgoubi/code/HEAD/tree/trunk/guide/Zgoubi.pdf>